ICAS 2016
30th Congress of the International Council of the Aeronautical Sciences
DCC, Daejeon, Korea ; September 25-30, 2016

EXPERIMENTAL AND SIMULATION STUDY OF THE DYNAMICS OF AN ELECTRO-MECHANICAL LANDING GEAR ACTUATOR

Gianpietro Di Rito*, Roberto Galatolo*, Francesco Schettini*
*** Università di Pisa - Dipartimento di Ingegneria Civile ed Industriale**

Abstract

This paper summarizes the testing and simulation activities carried out for the study of an electro-mechanical actuator for helicopter landing gear extension/retraction. The basic objective of the work was to obtain an experimentally-validated model of the actuator dynamics, to be used as support tool for the design enhancement as well as for the development of similar systems. The database for the model validation has been obtained by testing the actuator with a specifically developed real-time hardware-in-the-loop system, in which the actuator voltage supply is regulated by a programmable power unit, and its mechanical loading is controlled by a counteracting hydraulic servo. The test results in terms of actuator position, speed and motor currents, and related to different combinations of voltage supply and load factors, have been then used to tune the parameters of a model developed by the authors. The satisfactory matching between simulation predictions and experimental data allowed to highlight and discuss specific performance issues in the actuator speed response, which can be characterised by a limit-cycle behaviour when the landing gear is extended under high tensile loads.

1 Introduction

Electrification of onboard systems is nowadays one of the most important issues for engineers and researchers working on development of new aerospace vehicles. As pointed out in [1][2], a key point to achieve this strategic and challenging innovation is related to the development of Electro-Mechanical Actuators (EMA's) capable of adequate performances together with the required reliability/safety levels for airworthiness certification. In recent years, the topic has been deeply addressed, with focus on new design solutions for high-performance electric machines [3], reliable power electronics for motors [4], fault-tolerant architectures [5][6]. The technological novelty actually imposes to demonstrate the applicability of electro-mechanical actuators well before the manufacturing, so that a strong effort on modelling and simulation activities is required throughout the design phases [7][8]. As discussed in [9], when simulating electrical power systems for aerospace, a particular care must be paid on selecting the model complexity as function of the prediction objectives. Different approach can be thus followed, by obtaining models with increasing level of detail (*architectural*, *functional*, *behavioural* or *physical* models in [9]).

In this paper, the focus is on the development and experimental validation of the model of an EMA[1] for helicopter landing gear extension/retraction, to be used as support tool for the design enhancement and for the development of similar systems. The EMA model, characterised by a high level of detail, has been validated with a specifically developed real-time hardware-in-the-loop system, by characterizing its performances at different

[1] The EMA under exam has been developed by a team composed by Mecaer Aviation Group spa, Logic spa, and University of Pisa in the context of a project partially-funded by the Italian Ministry of Economic Development, within the frame of "Industria 2015-Nuove Tecnologie per il *Made in Italy*". Mecaer (project leader) was responsible for the mechanical/electrical design and manufacturing, Logic was in charge of the electronic control unit, while the University of Pisa supported the design with the development of actuator models.

operating conditions in terms of voltage supply and mechanical loadings.

2 System Description

The actuator under exam is an EMA for helicopter landing gear extension/retraction essentially composed of (Fig. 1):

- a 3-phase brushless DC motor (BLDCM);
- a mechanical transmission from the motor rotation to rod translation made of a two-stage epicyclical gearbox and a low-pitch planetary roller screw;
- an electromagnetic negative brake, used to block the motor shaft in the fully-retracted and fully-extended position;
- a mechanically-driven load disconnection device for the free-fall extension in emergency condition (free motion is obtained by manually removing a pre-loaded pin connecting the annular gears of the two stages of the gearbox);
- an automatic mechanically-driven lock device that holds the EMA in fully-extended position without loading the motor;
- an Actuator Control Unit (ACU) that provides the electrical supply to the motor coils via PWM drive, implements the closed-loop control of the motor speed, and manages the EMA operating modes (up, down, move-up, move-down).

3 Experimental Set-Up and Test Plan

3.1 Test System

The experimental activity for the model validation has been carried out by using a real-time/hardware-in-the-loop test system for aircraft actuators, developed and set-up within several research activities at the University of Pisa [10][11][12][13][14][15]. The system, specifically adapted for testing the reference EMA, is schematically depicted in Fig. 2. In the test system, the EMA is mounted on a hydraulic test bench (Fig. 3), and its test interfaces are managed as follows:

- the electrical interface is controlled by the PC Test 1, which, via LabView software, exchanges commands/feedbacks with the ACU and regulates the EMA voltage supply through a programmable power unit (HP 6032A, 0-60 V, 0-50 Amp, 1kW power limit, configurable via GPIB protocol)
- the mechanical loading is controlled by the PC Test 2, which, via Matlab-xPC Target software (the Host PC is not shown in Fig. 2), implements a closed-loop control of the force applied by the hydraulic servo of the bench. During the test, the hydraulic servo force demand varies in dependence on EMA position, in order to reproduce the load variation related to the landing gear extension/retraction kinematics (Fig. 1).

3.2 Test Plan

The experimental study aimed to characterize the EMA dynamics at different operative conditions, with particular reference to variation of vertical load factor (N_z) and supply voltage (V_{dc}). Four EMA operative conditions have been thus defined:

- *Nominal*: $N_z = 1$; $V_{dc} = 28$ V
- *Normal*: $N_z = 1.5$; $22\text{ V} \le V_{dc} \le 30.3\text{ V}$
- *Critical*:. $N_z = 3.5$; $20.5\text{ V} \le V_{dc} \le 32.2\text{ V}$
- *Limit*: $N_z = 3.5$; $V_{dc} = 14$ V

By selecting the extreme values of supply voltages for the ranges related to normal and critical conditions, a total of six test cases have been obtained.

This approach (i.e. no tests with intermediate values of voltage supply) has been chosen because the objective was not to provide a thorough and comprehensive description of the EMA dynamic behaviour, but to characterise the nominal response of the system and its maxima performance variations.

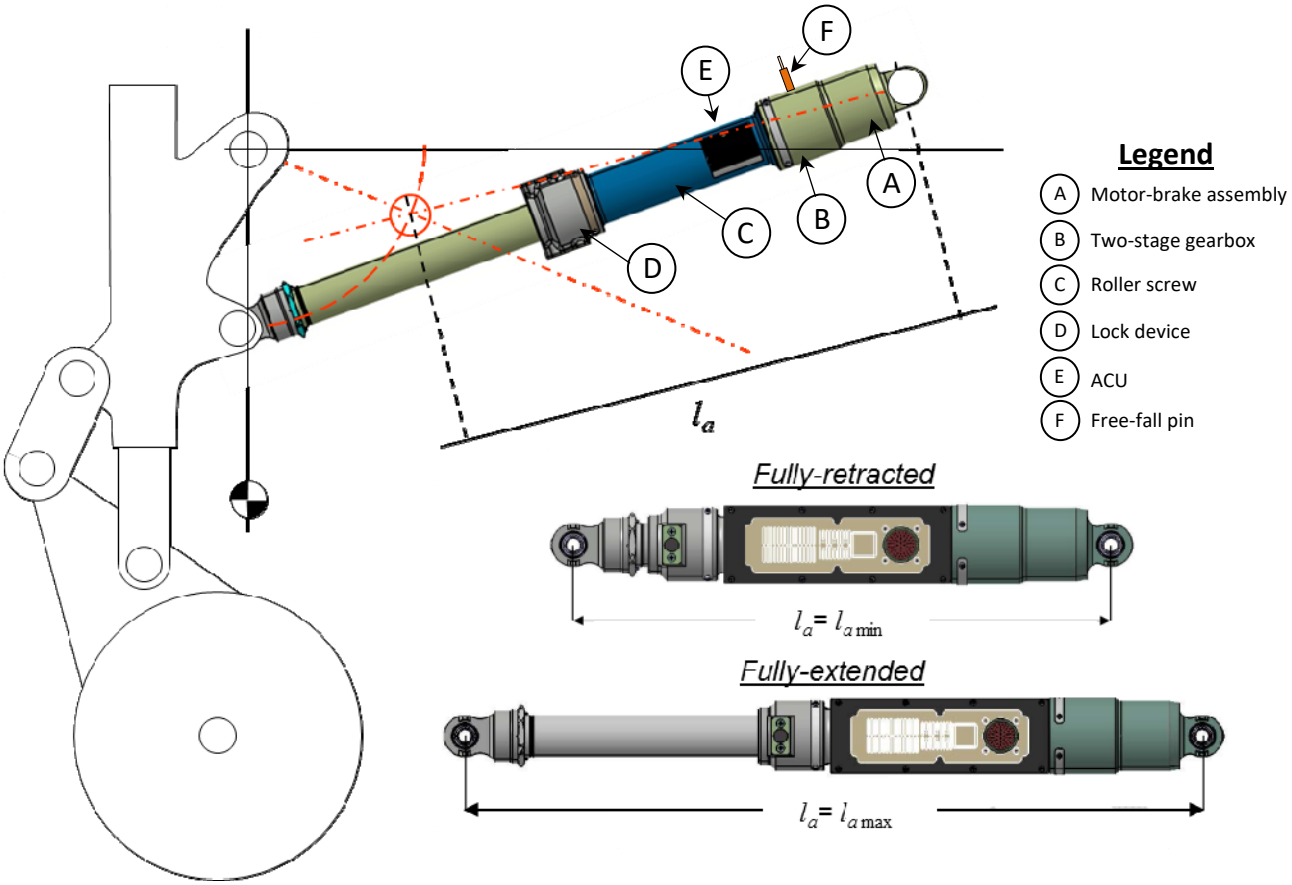

Fig. 1. Helicopter landing gear extension/retraction kinematics.

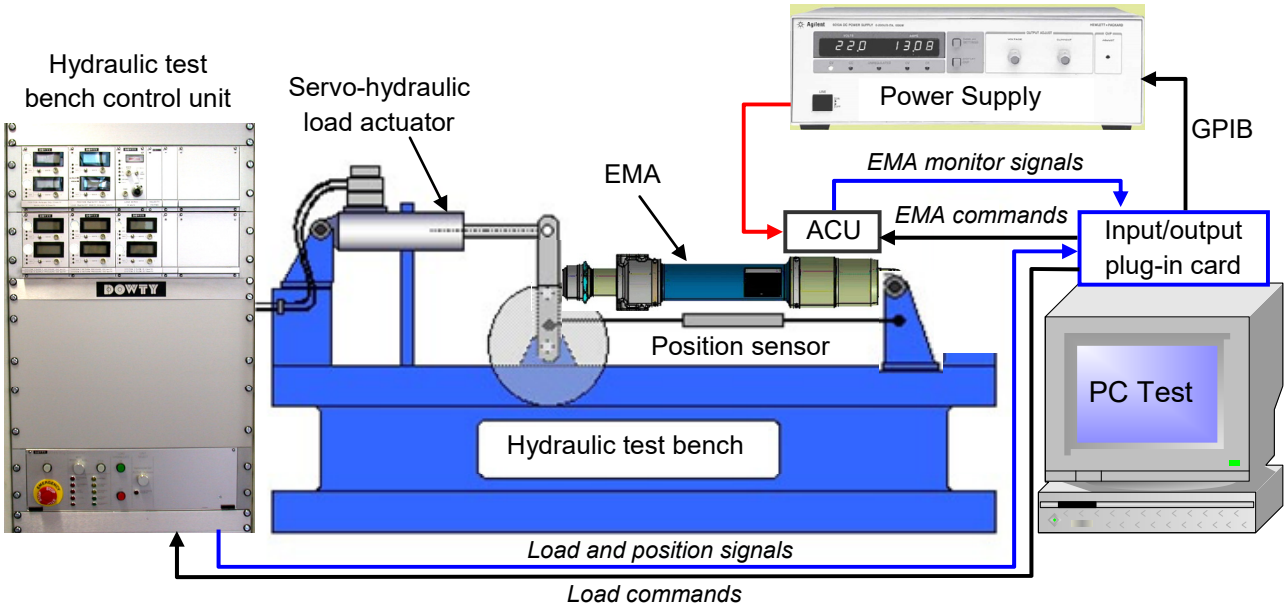

Fig. 2. Real-time/hardware-in-the-loop system for the EMA testing.

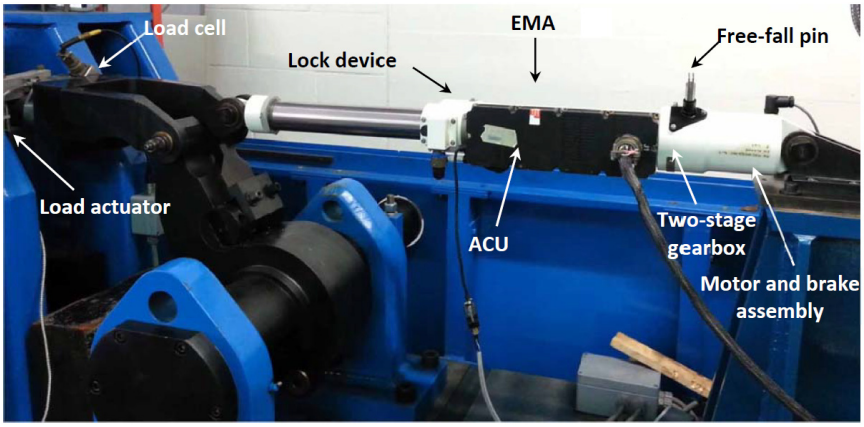

Fig. 3. EMA mounted on the test bench.

4 EMA model

4.1 Electrical motor

The three-phase BLDCM of the EMA has been modelled with reference to the scheme in Fig. 4, where one pole pair is shown to simplify the sketch.

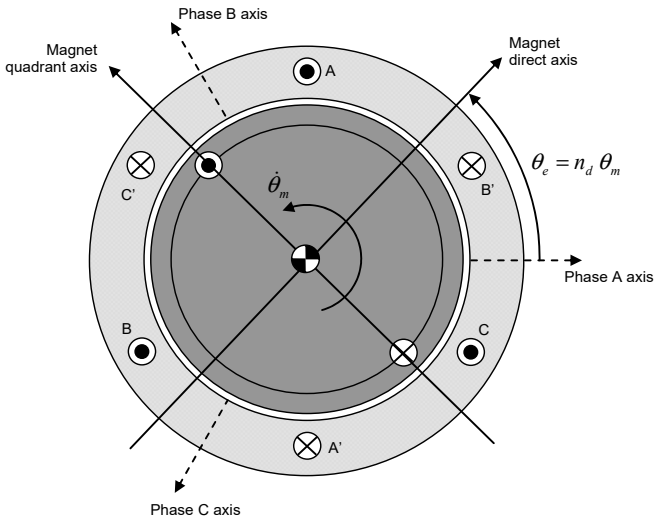

Fig. 4. Three-phase BLDCM schematics.

By assuming that the magnetic flux linkages of the phases are decoupled, we have

$$\boldsymbol{\lambda} = L\,\mathbf{i} + \lambda_m\,\mathbf{f_m} \qquad (1)$$

where L is the phase inductance, λ_m is the flux linkage due to the permanent magnets, while the the components of the vectors $\boldsymbol{\lambda}$, $\mathbf{i}$ and $\mathbf{f_m}$ represent the magnetic fluxes, the currents, and the magnetic flux shape functions of the three motor phases, respectively.

The current dynamics and the motor torque (T_m) are thus given by Eqs. (2)-(3),

$$\mathbf{V} = R\,\mathbf{i} + L\,\frac{d\,\mathbf{i}}{d\,t} + \lambda_m\,n_d\,\dot{\theta}_m\,\frac{d\,\mathbf{f_m}}{d\,\theta_e} \qquad (2)$$

$$T_m = \lambda_m\,n_d\,\frac{d\,\mathbf{f_m}}{d\theta_e}\cdot\mathbf{i} \qquad (3)$$

where n_d is the number of pole pairs, θ_m and θ_e are the mechanical and the electrical angle of the motor (Fig. 4), and $\mathbf{V}$ is the vector of the voltages applied to the phases. In BLDCM's, the phase windings are distributed along the stator in such a way that the components of the magnetic flux shape function vector ($\mathbf{f_m} = \left[f_{ma} \quad f_{mb} \quad f_{mc}\right]^T$) roughly behave as triangular waves with respect to the electrical angle, so that the resulting the back-electromotive force shape functions ($K_{ex} = df_{mx}/d\theta_e$, with x=a, b, c) are trapezoidal.

4.2 Control Electronics

4.2.1 Closed-loop speed control

In the reference application, the landing gear extension/retraction is obtained with a closed-loop control on the motor speed. A proportional-integrative regulator generates the electrical demand for the motor (V_{dem}) by elaborating the error between the demand speed (ω_{mi}) and the speed measurement (ω_{ms}), with a saturation at the nominal supply voltage for the integrative section of the regulator, Eqs. (4)-(6).

$$V_{dem} = K_{\omega P}(\omega_{mi} - \omega_{ms}) + V_{demI} \quad (4)$$

$$V_{demI} = \begin{cases} V_{s\max} & V_{demIns} \geq V_{s\max} \\ V_{demIns} & |V_{demIns}| < V_{s\max} \\ -V_{s\max} & V_{demIns} \leq -V_{s\max} \end{cases} \quad (5)$$

$$V_{demIns} = K_{\omega I}\int_0^t (\omega_{mi} - \omega_{ms})\,dt \quad (6)$$

Coherently with the digital signal processing performed by the ACU, the regulator in the EMA model is simulated by a discrete-time version of Eqs. (4)-(6), using at 100 Hz sampling frequency.

4.2.2 Voltage demands modulation

The model of the control electronics also includes the modulation of the voltage demands for the three phases (used to eliminate the torque dependence on the motor angle, Eq. (3)). This modulation, performed in the reference EMA by the ACU with three Hall-effect sensors, is simulated via the following demand shape functions:

$$K_{dem\,a}(\theta_e) = \begin{cases} 0 & 0 \leq \theta_e < \pi/6 \\ 1 & \pi/6 \leq \theta_e < 5\pi/6 \\ 0 & 5\pi/6 \leq \theta_e < 7\pi/6 \\ -1 & 7\pi/6 \leq \theta_e < 11\pi/6 \\ 0 & 11\pi/6 \leq \theta_e < 2\pi \end{cases} \quad (7)$$

$$K_{dem\,b}(\theta_e) = K_{dem\,a}(\theta_e - 2\pi/3) \quad (8)$$

$$K_{dem\,c}(\theta_e) = K_{dem\,a}(\theta_e + 2\pi/3) \quad (9)$$

so that, once an electrical demand is generated by the speed regulator (V_{dem} in Eq. (4)), the three phase voltage demands are given by

$$\mathbf{V_i} = V_{dem}\,\mathbf{K_{dem}} \quad (10)$$

4.2.3Power electronics

The simulation of the ACU logics for the electrical power drive is a key section of the developed EMA model. The power electronics logics derive from conventional BLDCM solutions with some specifically-designed modifications. In particular, the ACU uses two control modes:

a. Conventional Drive Mode (CDM), used when the electrical demand amplitude (V_{dem} , Eq. (4)) exceeds a predefined threshold V_{demTH} ;

b. Grounded Mode, implying that all the phases are grounded, and used when the electrical demand amplitude is lower than V_{demTH} .

In CDM, a set of three Hall sensors allows to define the 60-degree sector of electrical angle in which the motor is operating (six possible states from *State 0* to *State,* Table 1). For each operating sector, the six MOSFET's of the power bridge can be activated in conduction (i.e. set to *High*, H), deactivated (set to *Low*, L), or Pulse-Width Modulated (*PWM'd*) between H and L. The result is that, for each sector, the current is directed and regulated into only one couple of phases (the connection between the three phases and the power bridge is shown in Fig. 5, with the motor working at *State 0*).

The definition and use of the Grounded Mode has been necessary for the landing gear EMA to limit transient oscillations during the initial extension phase, in which high tensile loads are applied and the actuator must work as a brake for maintaining the speed demand. Actually, the MOSFET switching logics used in CDM (Table 1) implies that in *PWM'd* mode the voltage applied to the active couple of phases is switched between voltage supply and opened, so there are periods in the switching cycle in which the motor can freely rotate under the load, instead of acting as a brake.

Although more sophisticated power drive logics could be used (e.g. State-Vector PWM), this design approach has been chosen to simplify the system development and to limit the computing resources for the PWM drive, but it has also implied some drawbacks in terms of control performances, section 5.

MOSFET	*State 0* (0°<ϑ_e≤60°)	*State 1* (60°<ϑ_e≤120°)	*State 2* (120°<ϑ_e≤180°)	*State 3* (180°<ϑ_e≤240°)	*State 4* (240°<ϑ_e≤300°)	*State 5* (300°<ϑ_e≤360°)
Hi-side U	**H**	**H**	L	L	L	L
Lo-side U	L	L	L	**PWM'd**	L	**PWM'd**
Hi-side V	L	L	L	L	**H**	**H**
Lo-side V	L	**PWM'd**	**PWM'd**	L	L	L
Hi-side W	L	L	**H**	**H**	L	L
Lo-side W	**PWM'd**	L	L	L	**PWM'd**	L
Current flows from→to	U→W	U→V	W→V	W→U	V→W	V→U

Table 1. MOSFET switching logics in CDM.

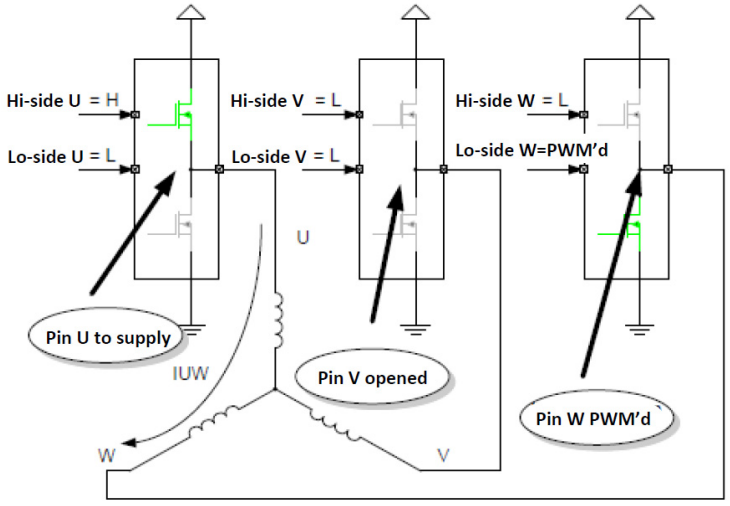

Fig. 5. Connection between motor phases and power bridge at *State 0* operation.

4.3 Mechanical section

4.3.1 Landing gear kinematics

The mechanical transmission from the motor shaft to the landing gear leg is supposed to be perfectly rigid, so that the EMA case rotation (β_a) and the screw translation with respect to EMA case (x_a) can be obtained as functions of the landing gear rotation (α_c) via Eqs. (11)-(12),

$$\begin{cases} \tan\beta_a = \dfrac{e_a + g_a \sin\alpha_c}{d_a - g_a \cos\alpha_c} \\ x_a = \dfrac{d_a - g_a \cos\alpha_c}{\cos\beta_a} - l_{a\min} \end{cases} \qquad (11)$$

$$x_a = f_x(\alpha_c) \quad \Rightarrow \quad \dot{x}_a = \frac{\partial f_x}{\partial \alpha_c}\dot{\alpha}_c = h_a\,\dot{\alpha}_c \qquad (12)$$

where $l_{a\min}$ is the EMA pin-to-pin length in fully-retracted position (x_a=0), h_a is the actuator horn radius and the other quantities are defined in Fig. 6.

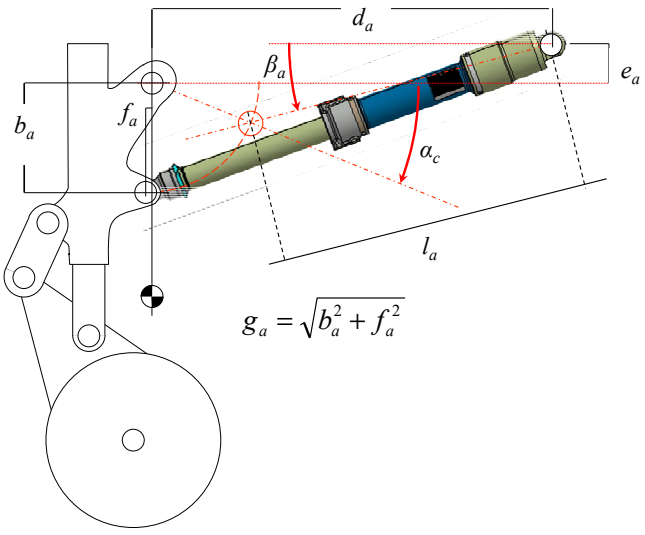

Fig. 6. Landing gear kinematics.

4.3.2 Momentum equation

By assuming a rigid mechanical transmission, the relationship between motor mechanical angle θ_m and rod displacement x_a is given by Eq. (13), and a unique momentum equation can be written for the whole landing gear, Eq. (14),

$$x_a = \frac{\theta_m \, p_s}{2\pi\,\tau_g} \tag{13}$$

$$J_{tot}\,\ddot{\theta}_m = T_m - T_c\,\mathrm{sgn}(\dot{x}_a) + T_{ext} \tag{14}$$

where J_{tot} is the equivalent system inertia, T_c is the velocity-dependant friction torque of the EMA, T_{ext} represents the torque contributions related to the external load, Eqs. (15).

$$\begin{cases} T_s = \dfrac{N_z F_{ext} p_s}{2\pi\,\tau_g}\left[1+\mathrm{sgn}(F_{ext}\,\dot{x}_a)\left(1-\dfrac{1}{\eta_a}\right)\right] \\ F_{ext} = f_F(x_a) \\ \eta_a = \eta_{a0}\, e^{-\sigma_F |F_{ext}|} + \eta_{a\infty} \end{cases} \tag{15}$$

In Eqs. (15), p_s is the screw pitch, τ_g is the two-stage gearbox ratio, F_{ext} is the external force applied to the rod, and η_a is the overall EMA direct efficiency. This last term mainly depends on the roller screw efficiency, which typically lowers with increasing loads [16]. For this reason, the EMA direct efficiency is assumed to depend on external force amplitude. Concerning the system inertia, it is calculated via Eq. (16), where m_n is the screw nut mass, h_a is the actuator horn radius, while J_l, J_m, J_s and J_g are the inertia of landing gear leg, motor, screw and gearbox respectively.

$$J_{tot} = J_m + \frac{J_s + J_g}{\tau_g^{\,2}} + \frac{p_s^{\,2}}{4\pi^2\tau_g^{\,2}}\left[m_n + \frac{J_l}{h_a^{\,2}}\right] \tag{16}$$

4.3 Model implementation, solver settings and numerical performances

The model, implemented in the Matlab-Simulink environment, demonstrated to provide numerically stable and affordable results using a fixed-step Runge-Kutta solver with 10^{-6} seconds integration step. On a common off-the shelf PC (Windows 7, CPU Intel Core i7-4770 3.4 GHz, 32 GB RAM), the ratio between computation time and simulation interval is about 1500.

5 Experimental Validation of the Model

A summary of the results obtained during the experimental validation of the model are reported from Fig. 7 to Fig. 10. The model is capable of reproducing the main characteristics of the EMA dynamics, even if enhancements are needed to simulate particular situations.

In extension at nominal condition, the initial acceleration is well simulated (Fig. 7) and the model succeeds in predicting the presence and the shape of a “hollow” in the speed response. This tracking anomaly appears for an interaction between the external load and the power electronics behaviour. In extension, the load promotes the EMA motion and the motor must act as a brake to maintain the speed demand. If the load is high, the power electronics operates with a *pulsating action*, by alternately switching from Grounded Mode to CDM with low duty cycle. In this condition, the motor phases pass from being grounded to be opened for significant periods, and the speed response is characterised by a limit-cycle. When the load lowers, the power electronics works with a *continuous action*, by applying a CDM with large duty cycles (i.e. the phases are more regularly driven and the motion is smoother). This complex dynamics can be also interpreted by the current results reported in Fig. 9, where the model predicts an anticipation of the transition to the *continuous action*, and the speed hollow is anticipated with respect to tests.

In retraction at nominal condition, the prediction is very good, Fig. 8. In this case, the external load counteracts the motion, the EMA acts as a motor, and the power electronics operates with *continuous action* throughout the stroke. Some errors are made in the initial phase, because the model does not simulate the lock device in fully-extended position.

Similar considerations can be made for the dynamics in normal conditions, which is here documented with reference to low voltage supply (less favourable). In extension, the power electronics operation with *pulsating action* is clearly observable in the model prediction, even if the transition to a *continuous action* is again anticipated with respect to experiments.

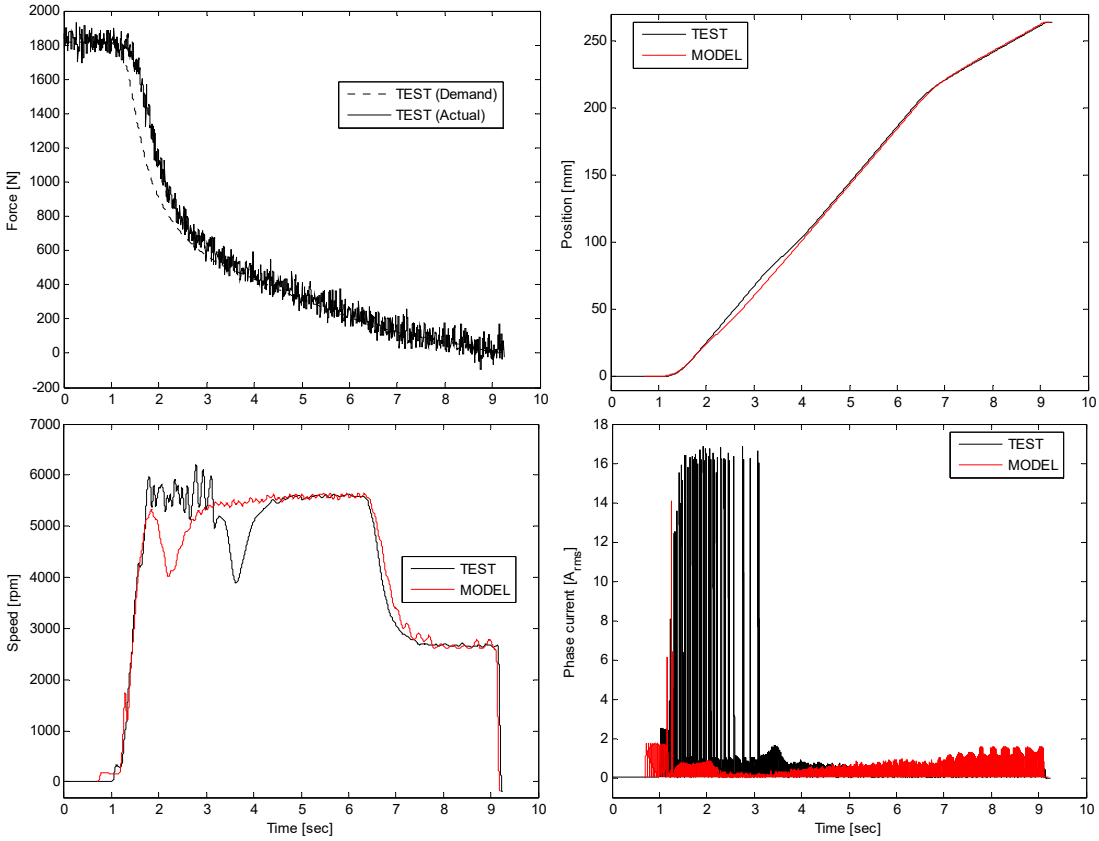

Fig. 7. Test and simulation results for extension at 28 V_{DC} and N_z = 1:
load tracking (up left), position response (up right) speed (down left), phase current (down right).

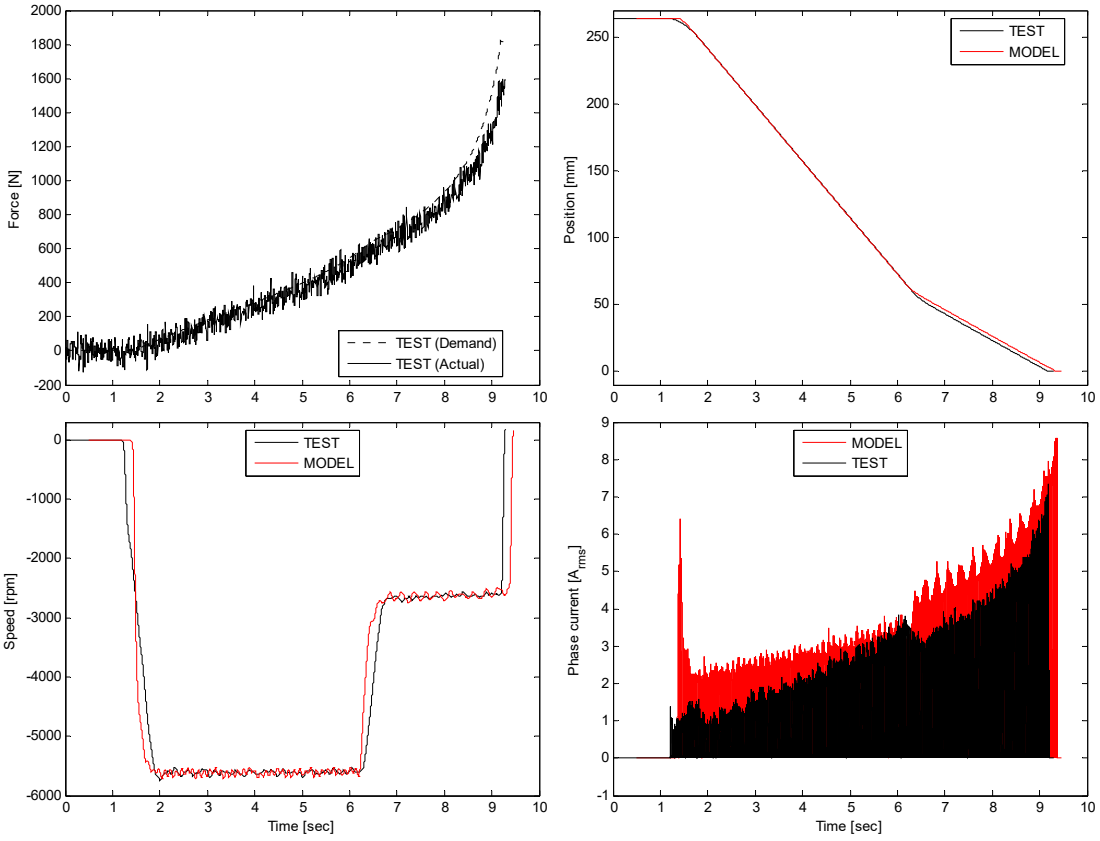

Fig. 8. Test and simulation results for retraction at 28 V_{DC} and N_z = 1:
load tracking (up left), position response (up right) speed (down left), phase current (down right).

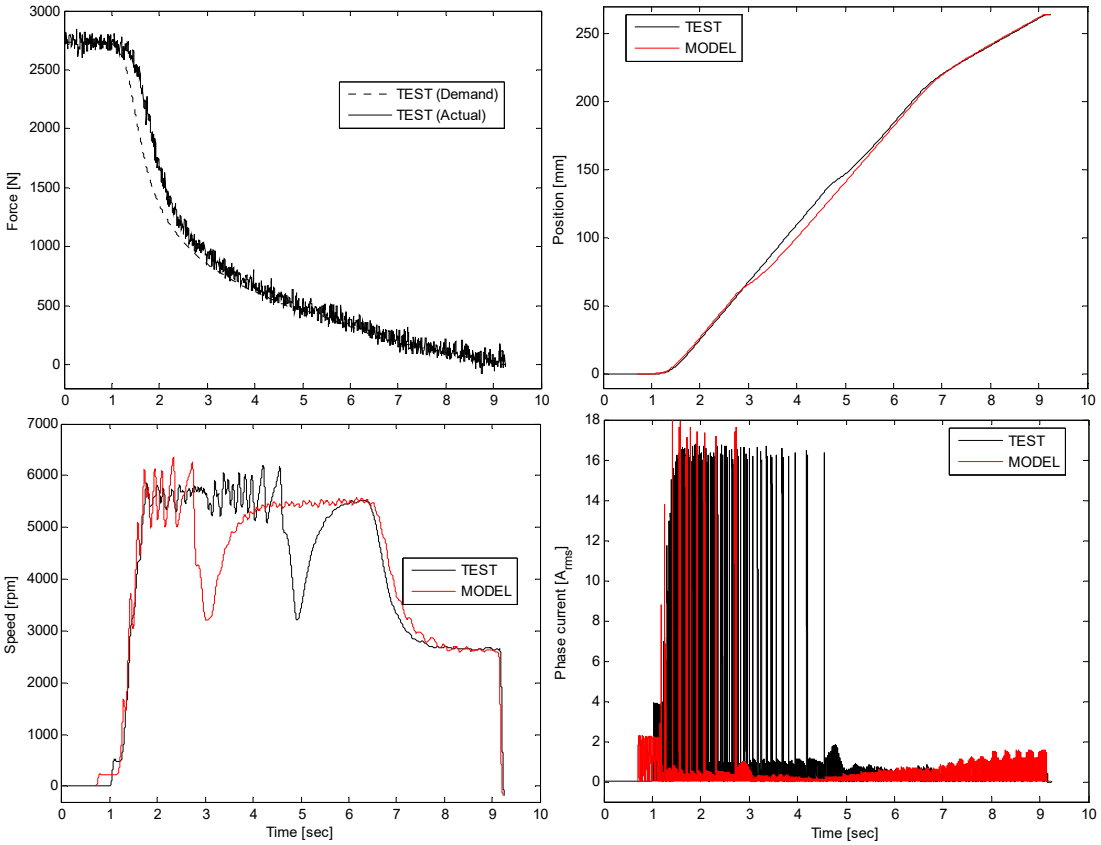

Fig. 9. Test and simulation results for extension at 22 V_{DC} and N_z = 1.5:
load tracking (up left), position response (up right) speed (down left), phase current (down right).

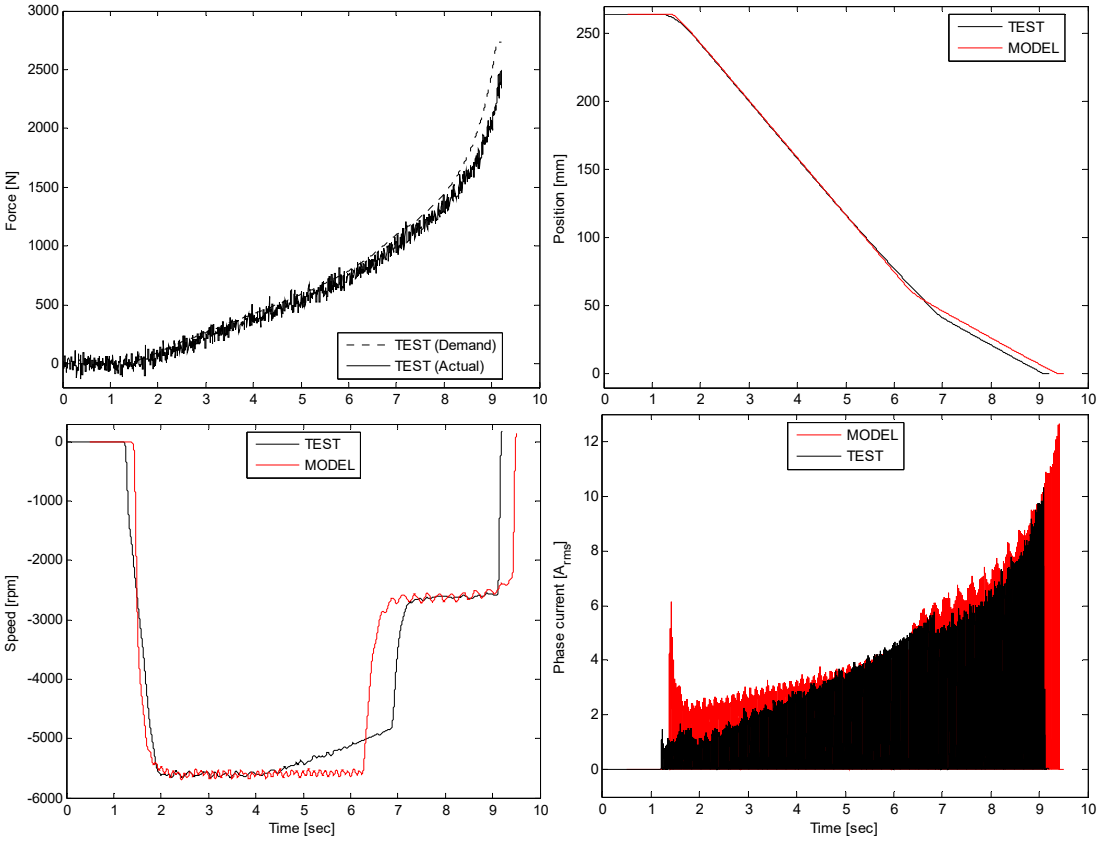

Fig. 10. Test and simulation results for retraction at 22 V_{DC} and N_z = 1.5:
load tracking (up left), position response (up right) speed (down left), phase current (down right).

Conclusions

The dynamics of a EMA for helicopter landing gear extension/retraction has been experimentally characterized by performing real-time hardware-in-the-loop simulations of operations at different levels of voltage supply and load factors. The test results have been compared with the simulation results of an EMA model, described in the paper and developed starting by physical principles. The model is capable of satisfactorily reproducing the experimental data in terms of position, speed and motor phase currents dynamics. In particular, the detailed modelling of the power electronics allowed to interpret and analyse some irregularities in the speed response during extension under high tensile loads, resulting in limit-cycle behaviours and degradations of speed tracking performances.

References

[1] Sarlioglu B., Morris C.T., *More Electric Aircraft: Review, Challenges, and Opportunities for Commercial Transport Aircraft*. IEEE Transactions on Transportation Electrification, Vol. 1, Issue 1, pp. 54-64, 2015.

[2] Rosero J.A., Ortega J.A., Aldabas E., Romeral. L., *Moving towards a more electric aircraft*. IEEE Aerospace and Electronic Systems Magazine, Vol. 22, Issue 3, pp. 3-9, 2007.

[3] Gerada C., Galea M., Kladas A., Electrical Machines for High Performance Aerospace Applications. *IEEE Workshop on Electrical Machines Design, Control and Diagnosis*, Turin (Italy), pp. 79-84, 2015.

[4] Garcia A., Cusido J., Rosero J.A., Ortega J.A., Romeral L., *Reliable Electro-Mechanical Actuators in Aircraft*, IEEE A&E Systems Magazine, 2008.

[5] Annaz F.Y., Fundamental design concepts in multi-lane smart electromechanical actuators. *Smart Materials and Structures*, Vol. 14, pp. 1227–1238, 2005.

[6] Di Rito G., Schettini F., Galatolo R., *Self-Monitoring Electro-Mechanical Actuator for Male Unmanned Aerial Vehicle Flight Controls*. Advances in Mechanical Engineering–Special Issue on Reliability for Aerospace Systems: Methods and Applications, Vol. 8(5) pp. 1–11, 2016.

[7] Di Rito G., Galatolo R., Denti E., Object-oriented modelling of flight control actuation systems for power absorption assessment. *Proc. of the 27th Congress of the International Council of Aeronautical Sciences (ICAS)*, Nice (France), 2010.

[8] Schettini F., Denti E., Di Rito G., Galatolo R., Simulation of an All-Electric Flight Control System for the Evaluation of Power Consumption. *Proceedings of the 29th International Council of the Aeronautical Sciences (ICAS)*, St. Petersburg (Russia), 2014.

[9] Wheeler P., Bozhko S., *The More Electric Aircraft: technology and challenges*, IEEE Electrification Magazine, Vol. 2, Issue 4, pp. 6-12, 2015.

[10] Di Rito G., Denti E., Galatolo R., Robust force control in a hydraulic workbench for flight actuators. *Proc. of the IEEE Joint Conference CCA, ISIC and CACSD*, Munich, Germany, 2006.

[11] Di Rito G., Denti E., Galatolo R., *Development and experimental validation of real-time executable models of primary fly-by-wire actuators*. Proc. of the Institution of Mechanical Engineers, Part I, Journal of Systems and Control Engineering, Vol. 222, Issue 6, pp. 523-542, 2008.

[12] Di Rito G., Galatolo R., *Experimental and theoretical study of the electrical failures in a fault-tolerant direct-drive servovalve for primary flight actuators*. Proc. of the Institution of Mechanical Engineers, Part I, Journal of Systems and Control Engineering, Vol. 222, Issue 8, pp. 757-769, 2008.

[13] Di Rito G., *Experiments and simulations for the study of temperature effects on the performances of a fly-by-wire hydraulic actuator*. Proc. of the Institution of Mechanical Engineers, Part I, Journal of Systems and Control Engineering, Vol. 225, I8, pp. 1195-1206, 2011.

[14] Di Rito G., Galatolo R., *Experimental assessment of the dynamic stiffness of a fault-tolerant fly-by-wire hydraulic actuator*, Proc. of the Institution of Mechanical Engineers, Part G, Journal of Aerospace Engineering, Vol. 226, n. 6, pp. 679-690, 2012.

[15] Di Rito G., Galatolo R., Denti E., Schettini F., Dynamic Notch Filtering Control for Fault-Tolerant Actuators of Fly-By-Wire Helicopters. *Proceedings of the 29th International Council of the Aeronautical Sciences (ICAS)*, St. Petersburg (Russia), 2014.

[16] Roller screws, SKF Publication 4351 EN - 2008-01.

Contact Author Email Address

g.dirito@dia.unipi.it

Copyright Statement